Demonstrating the Reverse Greenhouse Effect in the Laboratory – Part 2

Michael Schnell, Hermann Harde

1. Introduction

The ability of IR-active gases, the so-called Greenhouse(GH)-gases, to absorb thermal radiation is undeniable, as this has been demonstrated by countless infrared spectra. It is also widely agreed that Kirchhoff's radiation law also applies to GH-gases at high altitudes, where the spectral absorption is equal to the spectral emission (here , here). However, given the high collision rates of gas molecules at normal pressure, some authors assume that GH-gases in the lower atmosphere are not emitting and do not generate any counter- or back-radiation (here , here). Accordingly, excited GH-gases would only contribute to heat by collisions through radiationless deactivation (thermalization). In order to test the thermalization hypothesis and, if necessary, in the sense of K. Popper to refute this, a special apparatus was developed that simulates the principle of the negative GH-effect (see Part 1).

In an earlier experimental set-up, a heated and a cooled plate were housed together in a thermally insulated container. Experiments with this apparatus demonstrated that GH-gases can increase the back radiation, so that with constant heating the temperature of the warm plate (representing the Earth) is further increasing [1]. Any influence of GH-gases on the air temperature could not be observed in these studies, as there were hardly any changes. The effects of water vapor could also not be investigated, as this gas had to be removed to prevent condensation on the cold plate.

These disadvantages are overcome by a two-chamber arrangement. The focus is no longer on the Earth's temperature, but on the temperature of the atmosphere. In our actual experiments, the Earth's atmosphere is represented by a layer of warm air above a cooled plate. The air and plate are separated by a polyethylene (PE) foil, which suppresses any mechanical heat flows. Furthermore, the effects of water vapor can now be investigated, as the PE film prevents direct contact with the cold plate. As a radiation receiver, the cold plate enables an energy flow that can be interpreted as a simulation of heat transport both from the atmosphere toward the cooler Earth's surface and toward space.

The experiments show that even small amounts of a GH-gas are sufficient to significantly increase the thermal radiation of the air while simultaneously lowering its temperature. This demonstrates a negative GH-effect, which has the opposite effect to what is usually expected. We show on a laboratory scale and at an air pressure of the lower atmosphere that GH-gases can absorb the kinetic energy of their surrounding and convert it into thermal radiation through subsequent emission.

This detection is anything but simple, as a measurement with gases requires a cylinder as a container. And this is where the problems begin, because like all solid bodies, the cylinder emits thermal radiation. This so-called background radiation from the cylinder overlays the emissions of the GH-gases. As a result, only the tip of the gas radiation is visible, similar to an iceberg (see Part 1). This is also the reason why sophisticated, optimal experimental conditions are required to demonstrate this effect and why so many attempts have failed under these strict conditions. At first glance a horizontally positioned styrofoam box seems to be a convenient solution, as it is commercially available and easy to process. But as described in [2], such an experimental setup is unsuitable for detecting gas radiation, primarily because of its intense background radiation and also due to convection in the box.

2 . Experimental Set-Up

To examine how GH-gases affect the IR emission and temperature of an air parcel, all what you need is

a heated cylinder and a cooled blackened plate PC. To prevent convection, the warm cylinder is placed vertically on top of the cold PC plate, creating a stable stratification (see Fig. 1).

The real challenge is reducing the cylinder's background radiation. For this purpose, polished aluminum with a low emissivity of $\varepsilon \sim 5\%$ was used as the cylinder's surface (Fig. 1c). This does not look much, but the cylinder's inner surface is about ten times larger than the exit to the PC plate and thus, generates a background radiation of 78 W/m^2, while the radiance of CO_2 is about ten times lower.

The emitted IR radiation, commonly referred to as heat flow Q to the PC plate, is detected by two independent detectors: a small blackened disc on an insulating layer (detector TD) and ten mini-Peltier elements (detector VP) located directly on the PC plate (Fig. 1d).

As described in Part 1, in the air-filled cylinder, approximately 94% of the heat is dissipated by radiation transfer I_0 and 6% by mechanical heat conduction W_L. For simplicity, this heat flow Q is further referred to as background radiation I_0, although it contains a smaller amount of heat conduction.

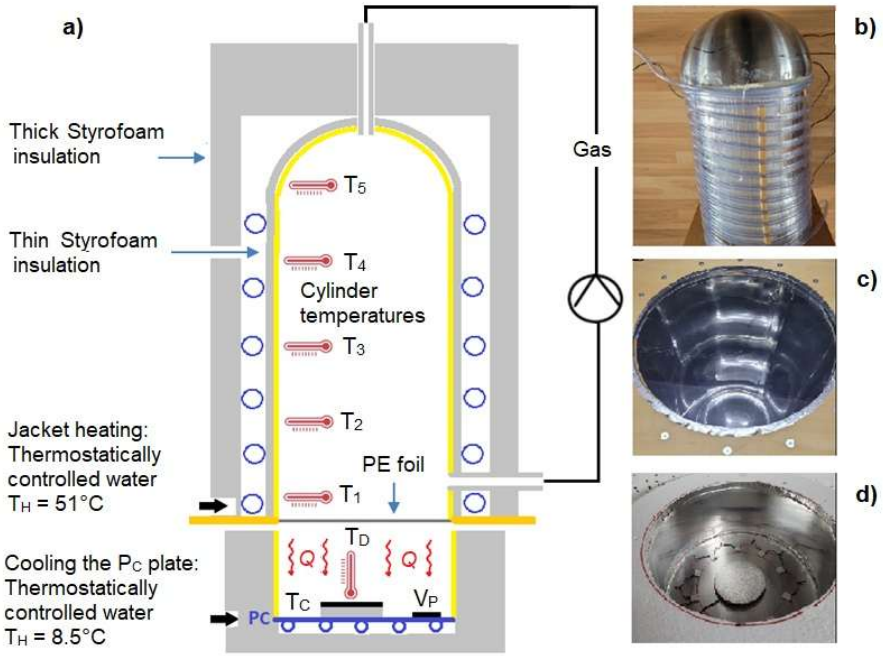

Fig. 1: a) Schematic experimental setup, b) gas cylinder with insulating wallpaper and PVC hose for the jacket heating TW, c) view into the interior of the gas cylinder with the PE foil, clamped between two wooden boards, d) plate PC with the thermal radiation sensors TD and VP, thermally insulated by a Styrofoam block with a mirrored aluminum inner wall.

In contrast, the additional heat flow, when adding GH-gases, consists exclusively of infrared radiation from the GH-gas. This follows also from the temperature changes with the difference $\Delta T_1 - \Delta T_C$, which become negative when adding the GH-gases. A positive increase in this difference would be essential for an increase in mechanical heat conduction (Equation 1, Part 1), but this is not observed (see Table 2b ff.). The differential measurement of the heat flow before and after addition of the greenhouse gas thus measures the pure gas radiation I_{Gas}. However, this is attenuated by superposition and transmission losses before it reaches the PC plate (Chapter 4).

The temperatures T_1 to T_5 are determined using temperature data loggers (Elitech). Since their measuring tip is only 5 cm from the cylinder wall, a mixture of air and wall temperature is measured, which is referred to as cylinder temperature. The investigation is concerned with these cylinder temperatures and their changes. For this reason, in contrast to the previous apparatus [1], the cylinder is not heated electrically, but rather with thermostatted water at 51 ± 0.1 °C. For this purpose, the warm water TW is continuously passed through the PVC hose of the jacket heater. Without outgoing heat flow Q, the cylinder and heating water temperatures should be almost the same. However, due to the heat flow, differences arise between the cylinder temperatures and the heating water temperature T_W (see Part 1). To

enhance this effect, a 2 mm thin layer of Styrofoam insulation was placed between the PVC hose and the cylinder wall. This weakens the heat flow from the water to the cylinder. Using this measure, the gas radiation I_{Gas} can also be easily detected by the temperature decrease after the addition of GH-gases (see Fig. 4 ff.).

The PC plate consists of a blackened aluminum sheet bonded to a spirally bent copper pipe in a concrete bed. Thermostatically controlled water flows through this pipe at a temperature of 10 ± 0.1 °C, continuously dissipating the absorbed heat.

3. Preparatory Studies

Extensive preparation is required to ensure that the effects found are actually identified as radiation of the IR-active gases and not as other influences.

To detect greenhouse gas emissions, a steady state with constant temperatures is required. This is achieved by circulating heated and temperature-controlled water through the cylinder jacket several hours before the start of the experiment and waiting until a steady state is established. For evaluation, an average value is determined one hour before and one hour after addition of a sample gas.

When this gas is colder than the air in the cylinder, the temperature drops briefly, especially in the T1 range (see Fig. 4 ff.). Blind tests using normal air as sample gas show that thermal equilibrium with the original temperatures has established again after just 20 minutes [3].

Thermal conductivity of the gases in the cylinder can be excluded, as experiments with the noble gases argon and helium show [3].

By calibrating with an external radiation source of known intensity, a strictly linear relationship is obtained for the two sensors TD and VP with an identical correlation coefficient of $R^2 = 0.999$ [3].

The respective radiation intensity can be calculated from the T_D and V_P values and the cross-section area $A = 0.0855$ m^2, whereby the average of both values is used to increase accuracy.

4. The Influence of Water Vapor on Background Radiation

To demonstrate the influence of water vapor, the cylinder temperatures T_1 to T_5 and the outgoing emission I_0 are measured at three different WV concentrations . The heating and cooling temperatures (T_W and T_C) are the same as those used in later GH-gas measurements.

The different WV concentrations, except for the T_1 measurement point, have minimal or no influence on the cylinder temperatures. This is due to the low WV concentration of only 1.9 vol.% compared to the other GH-gases (which were investigated at concentrations up to 8 vol.%) (see Part 1).

However, significant changes are seen in the background radiation I_0 , which increases from 79.4 to 85.1 W/m^2 with increasing humidity (Table 1).

Table 1: Measurements with air of different humidity.

W-Vapor %	T_1 °C	T_2 °C	T_3 °C	T_4 °C	T_5 °C	I_0 W/m^2	T_W °C	T_C °C
0.15	41.5	43.9	43.8	44.2	44.3	79.4	51.0	10.0
1.1	41.4	43.8	43.8	44.2	44.3	83.4	51.1	10.1
1.9	41.2	43.7	43.8	44.2	44.3	85.1	51.2	10.1

The measured values for this background radiation I_0 can be very well reproduced by radiation transfer calculations, when the background radiation from the cylinder walls and transmission losses are taken into account (Fig. 2).

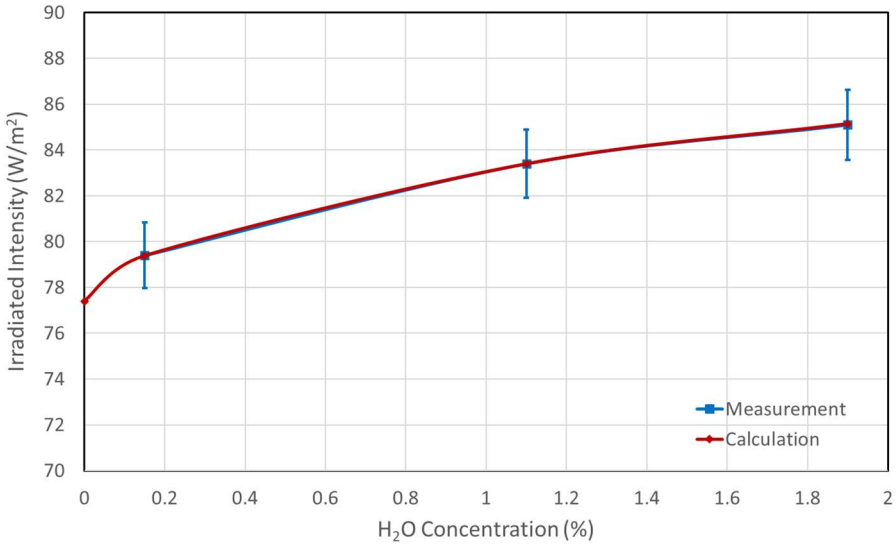

Fig. 2: Measured mean intensity (Rectangles, Blue) and calculated intensity (Diamonds, Red) of water vapor emission as a function of concentration at a background radiation by the cylinder of 77.4 W/m², for further details see Part 1.

According to these calculations, 0.15 vol.% water vapor inside the cylinder generate an additional radiation intensity of 10.5 W/m² . However, reaching the PC plate, this value drops to 2.0 W/m² . In the case of 1.9% WV, only 7.7 W/m² remain out of an expected WV intensity of 41.3 W/m².

These losses arise from the superposition of the WV radiation with the infrared radiation from the cylinder walls, as well as from transmission losses to the PC plate. The strong attenuations reveal the difficulties in experimentally detecting GH-gas radiation. Figure 3 shows that the WV bands (Blue lines) occupy the same wavenumbers as those of the background radiation from the cylinder walls (Gray dashed line), including the absorption lines of the PE foil at 750 and 1500 cm⁻¹. Due to these superpositions, only the WV intensities that exceed the gray line are effective.

The mutual superposition of the various greenhouse gases, especially with water vapor, occurs according to the same general principle:

The combined radiation of several greenhouse gases is always smaller than the sum of their individual contributions.

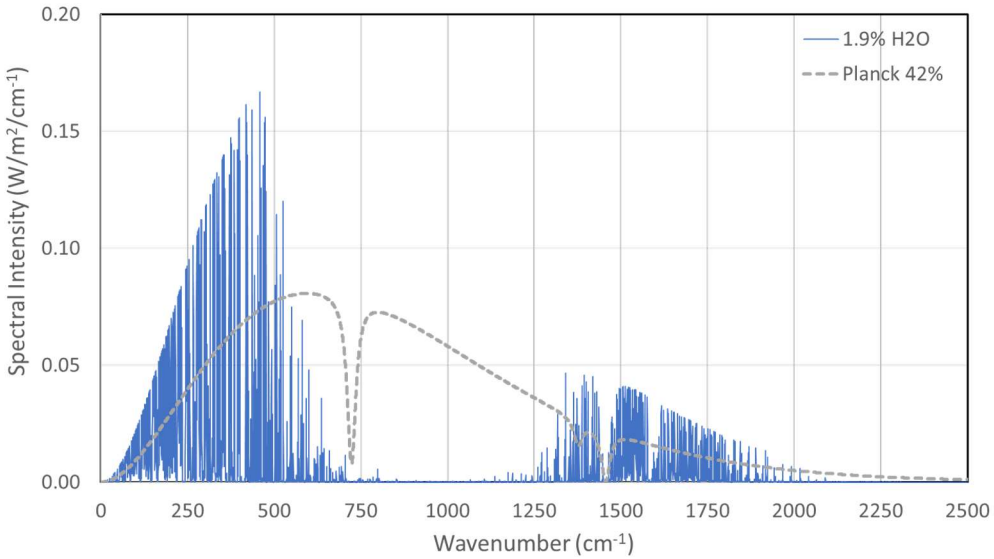

Fig. 3: Calculated intensity of 1.9% WV (Blue) and cylinder wall radiation (Grey, for ε = 42%) superimposed at the detector.

Within the atmosphere, there are further superpositions caused by aerosols and clouds. As Planck radiators with a continuous radiation spectrum, these solid and liquid particles can influence the emissions of all GH-gases. Therefore, the CO_2 GH-effect is significantly weaker under high humidity and overcast skies than under clear skies and low humidity.

The superposition of WV radiation with that of the other atmospheric greenhouse gases leads to a significantly reduced water vapor feedback. The IPCC assumes a positive feedback by a factor of 2–3 to inflate the effects of CO_2, thus forming the backbone of climate alarmism (here). Without this hypothesis, a doubling of the CO_2 concentration would only cause the Earth to warm by a harmless 0.6 to 1 °C (Harde 2013, 2014, 2017 [4 – 6]). Model calculations with a "water vapor feedback" assume so-called tropospheric hotspots, an increase in water vapor and temperature in the upper troposphere, between the equator and 30 degrees latitude. However, observational evidence for this hotspot has remained elusive, and subsequent analyses of radiosonde and satellite data have not confirmed the expected amplification in the tropical mid-troposphere, with some datasets showing trends inconsistent with model projections. See also the discussion in McKitrick & Christy (2018) [7]. Most of the warming since the 1970s has occurred near the surface (here).

5. The IR Emission of Greenhouse Gases

This section compiles the measurements and corresponding calculations for IR emission of the GH-gases CO_2, methane, nitrous oxide, and Freon 134a. All investigations are carried out at atmospheric pressure and constant initial temperatures. In addition to detecting IR radiation, the cooling of the gases, resulting from these emissions is also recorded.

The strongest cooling occurs at position T1 and gradually decreases towards the dome. This temperature gradient is consistent with radiation transfer according to the Schwarzschild equation and the layer model (Schwarzschild 1906 [8], Harde 2013 [4]). The T1 gas layer, located just 5 cm from the PE foil, can transfer its infrared radiation to the PC plate almost unhindered and cools down most strongly. All more distant layers must transport the energy through absorption and re-emission, resulting in attenuation with increasing distance from the PE foil. This effect is particularly evident with nitrous oxide and Freon, as these gases influence all five measuring points T1 – T5 (Subsections 5.1 and 5.4).

The intensity of the IR radiation reaching the PC plate is determined by the temperature or voltage increases of the TD or VP sensors and due to their calibration converted to W/m^2 [3].

I_0 is the background radiation of the experimental setup before, and I_G the total radiation intensity after addition of a GH-gas. By measuring the difference with and without GH-gases, the radiation component of the gas, $\Delta I_{Gas,}$ can be determined.

For control purposes, the changes in heating and cooling temperatures are also recorded as ΔT_W or ΔT_C. These values should be approximately zero to demonstrate that emissions and cylinder temperatures are not caused by external factors. This is entirely true for CO_2 and methane. For the stronger GH-gases nitrous oxide and especially Freon 134a, however, only the heating ΔT_W is approximately zero, while the cooling temperature T_C shows a significant increase of up to 0.7 °C, caused by the strong increase in gas radiation.

5.1. Freon 134a Radiation

Tetrafluoroethane (CF_2CF_3), also known as HFC-134a or Freon 134a, has been used for many years as a chlorine-free (not a CFC) efficient refrigerant. According to EU regulation, it is to be gradually phased out by 2030 on the basis of its measured GWP_{100} of approximately 1,430 – meaning its radiative forcing per molecule is substantially higher than CO_2 over a 100-year horizon. The present experiments confirm that this reflects real IR emission properties, not merely a theoretical construct.

Due to its strong GH-effect, Freon 134a is ideal for demonstrating gas radiation. A concentration of just 1 vol.% leads to an impressive increase in IR emission of 36 W/m² and a temperature reduction of the cylinder air of up to 2.8°C (see Fig. 4 and Table 2).

In view of these clear data, the thesis that greenhouse gases at normal pressure are only absorbers and do not emit infrared radiation or generate counter-radiation is clearly refuted.

Despite its strong effect, the effectiveness of Freon 134a also depends on the WV concentration. At a WV concentration of 1.1 vol.%, the radiation intensity is only about 88% of that of dried air (Table 2b).

Since Freon 134a is not listed as a line-by-line dataset in the HITRAN database, verification by radiation transfer calculations is not possible at this point.

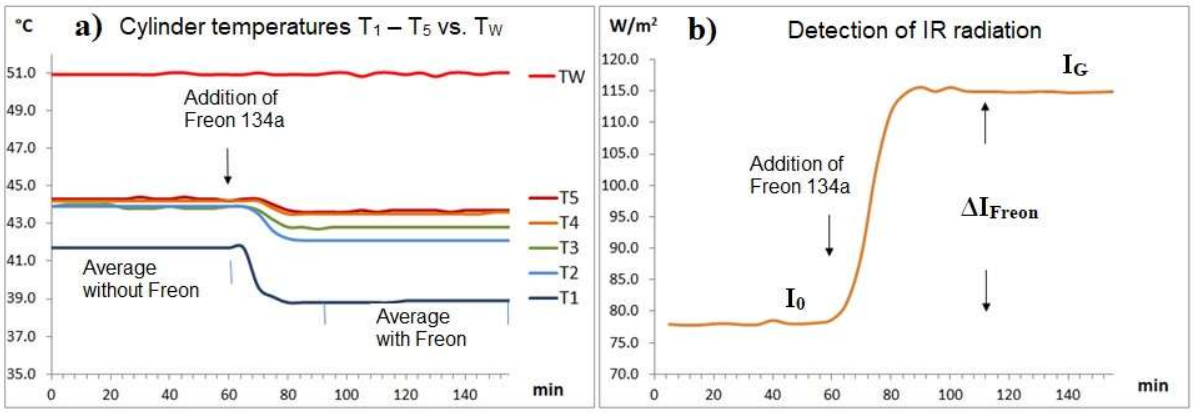

Fig. 4: Effects of 1% Freon 134a, a) decrease in cylinder temperatures, b) increase in IR radiation after addition of Freon, H_2O ~ 0.15 vol%.

Table 2a: Influence of Freon 134a and WV on the temperatures $T_1 - T_5$.

W-Vapor %	ΔT_1 °C	ΔT_2 °C	ΔT_3 °C	ΔT_4 °C	ΔT_5 °C	ΔT_W °C	ΔT_C °C
Freon: 1%							
0.1% H2O	-2.8	-1.8	-1.1	-0.7	-0.6	0.0	0.6
1.1% H2O	-2.4	-1.5	-0.9	-0.6	-0.5	0.0	0.5
Freon: 2 %							
0.1% H2O	-3.1	-1.9	-0.9	-0.4	-0.5	0.1	0.7
1.1% H2O	-2.7	-1.6	-0.7	-0.3	-0.3	0.0	0.6
Freon: 4 %							
0.1% H2O	-3.5	-1.8	-0.8	-0.3	-0.2	0.0	0.7
1.1% H2O	-3.0	-1.5	-0.5	-0.2	-0.1	0.0	0.6

Table 2b: Measurement of IR intensities before and after addition of Freon 134a. ΔI_{Freon} = Change of Intensity due to Freon radiation.

W-Vapor %	I_0 W/m²	I_G W/m²	ΔI_{Freon} W/m²
Freon: 1%			
0.15% H2O	78.3	114.9	36.6
1.1% H2O	82.7	114.8	32.1
Freon: 2%			
0.15% H2O	77.3	117.4	40.1
1.1% H2O	83.4	119.0	35.6
Freon: 4%			
0.15% H2O	76.9	119.4	42.5
1.1% H2O	83.4	120.2	36.8

5.2. CO_2 Radiation

The effectiveness of CO_2 is much weaker than that of Freon. Therefore, as with the following GH-gases, higher concentrations of 2, 4, and 8 vol.% are used. At these concentrations, the addition of CO_2 leads to a noticeable cooling of the T_1 and T_2 temperatures with a simultaneous increase in the IR radiation intensity ΔI_{CO2} (Fig. 5).

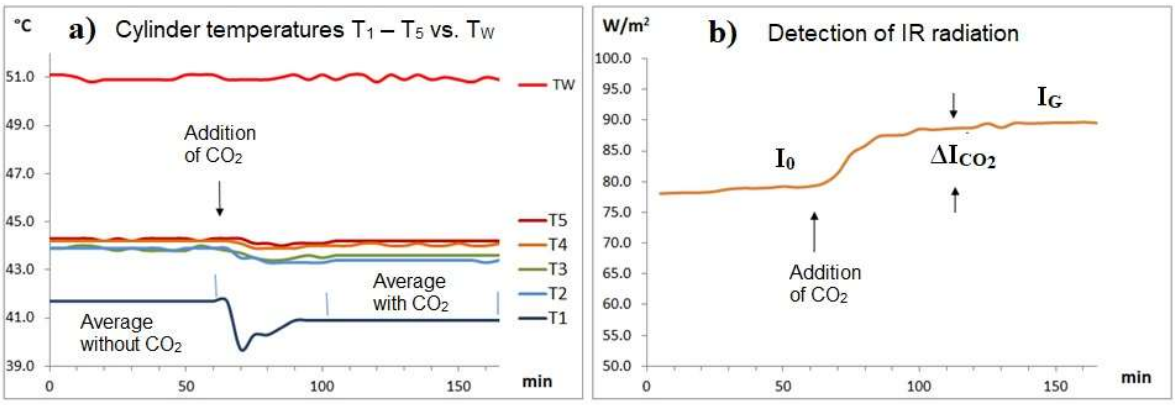

Fig. 5: Effects of 8 vol.% CO_2, a) decrease in cylinder temperatures, b) increase in IR radiation after addition of CO_2 (H_2O ~ 0.15%).

Note: Due to the significantly lower effect compared to Freon 134a, the diagrams for CO_2, methane and nitrous oxide are each shown at 8 vol.%.

Table 3a: Influence of CO_2 and WV on temperatures $T_1 - T_5$.

W-Vapor %	ΔT_1 °C	ΔT_2 °C	ΔT_3 °C	ΔT_4 °C	ΔT_5 °C	ΔT_W °C	ΔT_C °C
CO2: 2%							
0.15% H2O	-0.5	-0.5	-0.2	-0.2	-0.1	0.0	0.1
1.1% H2O	-0.4	-0.3	-0.2	-0.2	-0.1	0.0	0.1
1.9% H2O	-0.3	-0.3	-0.2	-0.1	-0.1	0.0	0.1
CO2: 4 %							
0.15% H2O	-0.6	-0.6	-0.4	-0.2	-0.2	0.0	0.1
1.1% H2O	-0.5	-0.3	-0.2	-0.1	-0.1	0.0	0.1
1.9% H2O	-0.4	-0.3	-0.2	-0.1	-0.1	0.0	0.1
CO2: 8 %							
0.15% H2O	-0.8	-0.5	-0.3	-0.2	-0.1	0.0	0.2
1.1% H2O	-0.5	-0.4	-0.2	-0.1	-0.1	0.0	0.2
1.9% H2O	-0.4	-0.4	-0.2	-0.1	0.0	0.0	0.2

In the case of CO_2, the influence of water vapor is examined at three concentrations (0.15%, 1.1%, and 1.9 vol%) (Tables 3a and 3b). With increasing WV concentration, it is shown that the background radiation continues to increase, leading to a weakening of the CO_2 radiation component. This weakening is particularly noticeable at lower concentrations of WV and CO_2, as shown by the different gradients after the addition of CO_2. For example, an H_2O concentration of 0.15 % results in an increase of 7.7 W/m², whereas for 1.9% WV the increase is only 5.7 W/m² (see Table 3b, last column). This is only 74% of the original intensity. The weakening is due to an increase in the background and thus an increased saturation of the CO_2 flanks.

Table 3b: Measurement of IR intensities before and after addition of CO_2 .

W-Vapor %	I_0 W/m²	I_G W/m²	ΔI_{CO2} W/m²
CO2: 2 %			
0.15% H2O	81.7	89.4	7.7
1.1 % H2O	83.9	89.8	5.9
1.9 % H2O	85.4	91.1	5.7
CO2: 4 %			
0.15% H2O	79.4	88.2	8.8
1.1 % H2O	82.9	90.2	7.3
1.9 % H2O	84.6	91.1	6.5
CO2: 8 %			
0.15% H2O	78.8	89.3	10.5
1.1 % H2O	82.6	90.9	8.3
1.9 % H2O	84.8	92.5	7.7

For verification, the measured data for the total intensity I_G are compared with radiative transfer calculations for CO_2 and H_2O (Fig. 6, Mea = Measured, Cal = Calculated). Details of these calculations, which are also available for methane and nitrous oxide, can be found in [3].

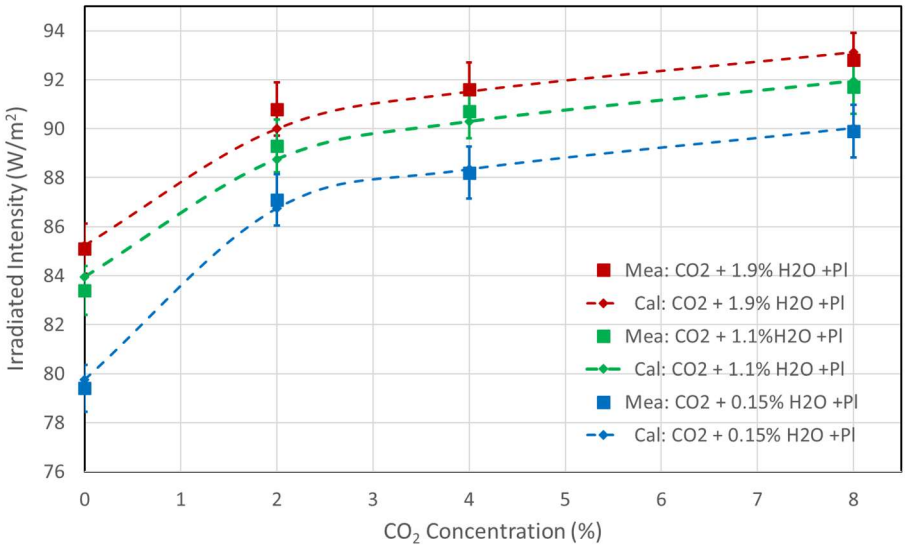

Fig. 6: Measurements (squares with error bars) and calculations (rhombuses, dashed line) for the IR radiation of CO_2 at different WV concentrations (0.15% Blue, 1.1% Green, 8% Red) and background radiation through cylinder walls PI.

However, due to the long propagation paths in the atmosphere and the 30 – 40 times higher WV concentration compared to CO_2, the weak overlap of the spectra around 670 cm^{-1} (part 1, Fig. 2) leads to a significant limitation of the CO_2 climate sensitivity and also to a reduced water vapor feedback (Harde 2014 [5], Harde 2017 [6]).

The different increase in the CO_2 radiation intensity at concentrations below and above 2% is striking, changing from an almost linear to a logarithmic curve and reflecting the clear saturation of the absorption and emission processes in the main band around 670 cm^{-1}. For concentrations above 2%, the further increase in intensity is primarily determined by the unsaturated wings and weaker bands.

This phenomenon of a "kink" in the increase in radiation intensity can be observed for all greenhouse gases. This change in sensitivity is the reason why the so-called "global warming potential," the comparison of a greenhouse gas at very low concentrations with CO_2, is a comparison of apples and oranges (see methane).

5.3 Methane radiation

Fig. 7 displays a measurement for 8 vol.% of CH_4 in dry air. Methane is considered as a particularly dangerous greenhouse gas because, depending on the timescale, it is said to have a global warming potential 25 to 84 times higher than CO_2. This classification paradoxically arises from its low atmospheric concentration of approximately 2 ppm. In this range, the optical density is still very low compared to CO_2, so there is a linear increase in the potential. CO_2, on the other hand, at 420 ppm, is already in the logarithmic range (see Chapter 5.2). The completely different spectral overlaps with water vapor are another reason for the accusation of "apples and oranges" (see Part 1, Fig. 2).

Global warming potential is often mistakenly confused with effectiveness. In fact, based on equal concentrations, methane is a weaker greenhouse gas than CO_2 (Table 4b vs. Table 3b). Theoretical calculations (Part 1, Chapter 2) have already shown that the IR radiation of methane is lower than that of CO_2. This has now been confirmed by experiments. Methane is oxidized to CO_2 in the atmosphere under the influence of ozone and UV light and therefore has a relatively short residence time of approximately 9 to 12 years.

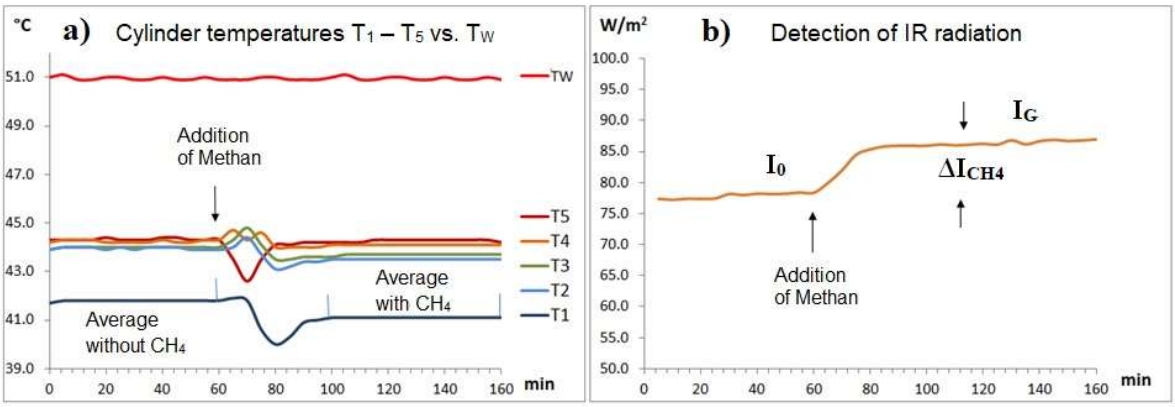

Fig. 7: Effects of 8 vol.% methane, a) decrease in cylinder temperatures, b) increase in IR radiation after addition of CH_4, H_2O ~ 0.15 vol.%.

Table 4a: Influence of CH_4 and WV on the gas temperatures $T_1 - T_5$.

W-Vapor %	ΔT_1 °C	ΔT_2 °C	ΔT_3 °C	ΔT_4 °C	ΔT_5 °C	ΔT_W °C	ΔT_C °C
CH4: 2%							
0.15% H2O	-0.5	-0.4	-0.1	-0.1	0.0	0.0	0.1
1.1% H2O	-0.2	-0.2	-0.1	-0.1	0.0	0.0	0.1
CH4: 4%							
0.15% H2O	-0.5	-0.4	-0.3	-0.2	-0.1	0.0	0.1
1.1% H2O	-0.4	-0.3	-0.2	-0.1	0.0	0.0	0.1
CH4: 8%							
0.15% H2O	-0.7	-0.5	-0.3	-0.1	-0.1	0.0	0.2
1.1% H2O	-0.6	-0.3	-0.2	0.0	0.0	0.0	0.1

Table 4b: Measurement of IR intensities before and after addition of CH_4. ΔI_{CH4} = intensity change due to CH_4 radiation.

WD %	I_0 W/m²	I_G W/m²	ΔI_{CH4} W/m²
CH4: 2 %			
0.15% H2O	78.6	84.9	6.3
1.1 % H2O	80.8	84.8	4.0
CH4: 4 %			
0.15% H2O	78.4	85.0	6.6
1.1 % H2O	80.9	86.8	5.9
CH4: 8 %			
0.15% H2O	78.0	86.5	8.5
1.1 % H2O	85.3	92.1	6.8

As with CO_2, methane radiation also depends on the water vapor concentration. The greatest methane effect is found at a H_2O concentration of 0.15 vol.% and is only 78% of the original effect at 1.1% water vapor (Table 4b).

5.4 Nitrous Oxide Radiation

Nitrous oxide (N_2O, laughing gas), the third most important long-lived greenhouse gas, is thought to contribute significantly to global warming due to its long atmospheric residence time and its greenhouse potential, which is approximately 300 times higher than that of CO_2. In radiation experiments, the effect of N_2O is noticeably greater than that of CO_2, but only by a factor of 1.5 at the same concentration (Table 5b vs. Table 3b). Even in theoretical calculations, the IR radiation of nitrous oxide is only slightly higher than that of CO_2 (Part 1, Chapter 2).

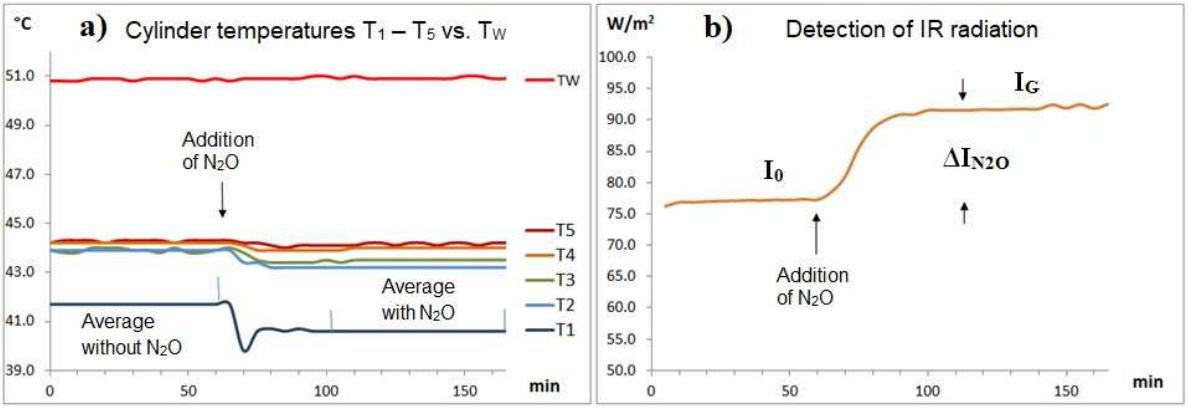

Fig. 8: Effects of 8 vol.% nitrous oxide, a) decrease in cylinder temperatures, b) increase in IR radiation after addition of N_2O at a WV concentration of 0.15%.

Table 5a: Influence of N_2O and WV on the gas temperatures $T_1 - T_5$.

W-Vapor %	ΔT_1 °C	ΔT_2 °C	ΔT_3 °C	ΔT_4 °C	ΔT_5 °C	ΔT_W °C	ΔT_C °C
N2O: 2%							
0.15% H2O	-0.7	-0.6	-0.4	-0.3	-0.2	0.0	0.2
1.1% H2O	-0.5	-0.5	-0.2	-0.2	-0.1	0.0	0.2

N2O: 4 %							
0.1% H2O	-0.9	-0.7	-0.4	-0.3	-0.2	0.0	0.2
1.1% H2O	-0.7	-0.5	-0.3	-0.2	-0.2	0.0	0.2
N2O: 8 %							
0.1% H2O	-1.1	-0.7	-0.4	-0.2	-0.1	0.1	0.3
1.1% H2O	-0.8	-0.6	-0.3	-0.2	-0.1	0.0	0.2

Table 5b: Measurement of IR intensities before and after addition of N_2O. ΔI_{N2O} = intensity change due to N_2O radiation

W-Vapor %	I_0 W/m²	I_G W/m²	ΔI_{N2O} W/m²
N2O: 2 %			
0.15 % H2O	79	89.7	10.7
1.1 % H2O	83.8	92.9	9.1
N2O: 4 %			
0.15 % H2O	77.3	89.8	12.5
1.1 % H2O	84.8	95.8	11
N2O: 8 %			
0.15 % H2O	77.1	91.9	14.8
1.1 % H2O	85.2	97.7	12.5

With 0.3 ppm, the concentration of N_2O in the atmosphere is 1400 times lower than that of CO_2 , raising questions about its effectiveness.

As with CO_2 and CH_4, nitrous oxide radiation also depends on the water vapor concentration. The greatest effect is again achieved at an H_2O concentration of 0.15 vol.% and is reduced to 86% of the original effect at 1.1% water vapor (Table 5b).

6. Summary

This study was performed to demonstrate, on the one hand, the emission properties of greenhouse gases under conditions similar to those in the lower atmosphere and, on the other hand, to demonstrate the existence of the negative GH-effect on a model scale.

For this purpose, a two-chamber vertical set-up was developed. The upper part of this apparatus is a heated gas cylinder, and the lower part is a thermally insulated cylinder with a cooled plate containing thermal radiation detectors.

CO_2, methane, or nitrous oxide are added to the upper cylinder and dependent on their concentration, a decrease in air temperatures and a simultaneous increase in IR radiation are observed. This means that these GH-gases can absorb the kinetic energy of their surroundings through inelastic collisions with other air molecules and convert this energy into thermal radiation through subsequent emission.

A cooling of the air accompanied by an increase in thermal radiation is called the "negative GH-effect," since it is usually the other way around. Such reversals are also part of the Earth's climate system in inversion weather conditions, the nighttime cooling of the air near the ground, or the air currents toward the winter poles.

The theory that a GH-effect is fundamentally impossible, since collision processes supposedly lead to radiationless deactivation and thus no back radiation, is refuted by these experiments. In the case of only thermalization, the effects of GH-gases would have to be exactly the opposite, because then the air would have to warm up, and attenuating the IR emission, which was not observed.

Although the water vapor concentration can only be increased to a limited extent due to its tendency to condense, a significant attenuation of the effects of the above-mentioned GH-gases was observed in the presence of water vapor.

The often erroneously cited theory that gas radiation violates the second law of thermodynamics does not hold in these studies, as they only consider the heat flow from warm to cold. This eliminates a fundamental argument of the skeptics.

A plausibility check using radiation transfer calculations shows good agreement with the measured data when unavoidable losses are taken into account.

Detecting the gas radiation is anything but simple, as the background radiation from the upper cylinder masks the radiation from the GH-gases, making only a fraction of their radiation visible. Detecting these attenuated effects requires sophisticated technology. In addition to mirrored surfaces, a vertical experimental setup that prevents convection is a minimum requirement.

References

1. H. Harde, M. Schnell, 2022: *Verification of the Greenhouse Effect in the Laboratory* , Science of Climate Change, Vol. 2.1, 1- 33. https://doi.org/10.53234/scc202203/10
2. M. Schnell, H. Harde, 2025: *The Negative Greenhouse Effect Part I: Experimental Studies with a Common Laboratory Set-Up* , Science of Climate Change, Vol. 5.3., pp. 1-9, https://doi.org/10.53234/scc202510/ 02 .
3. H. Harde, M. Schnell 2025: *The Negative Greenhouse Effect Part II: Studies of Infrared Gas Emission with an Advanced Experimental Set-Up* , Science of Climate Change, Vol. 5.3., pp. 10-34, https://doi.org/10.53234/scc202510/03 .
4. H. Harde, 2013: *Radiation and Heat Transfer in the Atmosphere: A Comprehensive Approach on a Molecular Basis* , International Journal of Atmospheric Sciences (Open Access), vol. 2013, http://dx.doi.org/10.1155/2013/503727
5. H. Harde, 2014: *Advanced Two-Layer Climate Model for the Assessment of Global Warming by CO_2*, Open Journal of Atmospheric and Climate Change, Vol. 1.3, November 2014, https://web.archive.org/web/20160429061756/http://www.scipublish.com/journals/ACC/papers/download/3001-846.pdf .
6. H. Harde, 2017: *Radiation Transfer Calculations and Assessment of Global Warming by CO_2,* International Journal of Atmospheric Sciences, Volume 2017, Article ID 9251034, pp. 1-30, https://doi.org/10.1155/2017/9251034 .
7. K. Schwarzschild, 1906: *Über das Gleichgewicht der Sonnenatmosphäre*. In: Nachrichten von der Königlichen Gesellschaft der Wissenschaften zu Göttingen, Mathematisch-Physikalische Klasse, 1906, Heft 1, pp. 41–53 (13. January 1906).
8. R. McKitrick, J. Christy, 2018: *A Test of the Tropical 200- to 300-hPa Warming Rate in Climate Models*, Earth and Space Science, 5, 529–536, https://doi.org/10.1029/2018EA000401